minerals

Article

Impact of Lithologic Heterogeneity on Brittleness of Cenozoic Unconventional Reservoirs (Fine-Grained) in Western Qaidam Basin

Xiang Li [1,2,*], Kunyu Wu [3,4], Jiangong Wang [2], Shaoyong Yang [4], Qinghui Zhang [4] and Qiang Zhang [2]

[1] School of Geoscience and Technology, Southwest Petroleum University, Chengdu 610500, China
[2] PetroChina Research Institute of Petroleum Exploration & Development-Northwest, Lanzhou 730020, China
[3] School of Petroleum and Natural Gas Engineering, Southwest Petroleum University, Chengdu 610500, China
[4] Research Institute of Exploration and Development of PetroChina Qinghai Oilfield Company, Dunhuang 736202, China
* Correspondence: lixiang1990@petrochina.com.cn

Abstract: In order to understand the impact on reservoir brittleness of lithologic heterogeneity in the continental mixed fine-grained sedimentary rocks in the western Qaidam Basin, the mechanical properties of the rocks and their correlation with mineral composition and petrographic characteristics were studied. A total of 20 samples from two parallel groups (10 samples in each group) were analyzed by triaxial stress test mineralogy, and morphology. The results show that the reservoir rocks can be divided into five different types according to the mechanical properties of the reservoir (characterized by stress–strain curves), among which Types I and III belong to a similar elastoplastic failure model, Type II shows a special pulse failure mode for plastic material, Type IV shows a failure mode of mixed characteristics, and Type V exhibits a typical plastic failure model. The correlation between minerals and mechanical properties indicates that quartz and feldspar, which are often considered brittle minerals, do not contribute much to the brittleness of these continental fine-grained sedimentary rocks. The main minerals affecting the reservoir brittleness are dolomite and clay minerals, contributing positively and negatively to it, respectively. The petrographic analysis results prove that the abnormal correlation between rock mechanical properties and quartz and feldspar is caused by the different rock fabrics. When dolomite forms a rock skeleton, it typically exhibits greater strength, brittleness and physical properties than other minerals. Based on the results, a brittleness evaluation standard for continental unconventional reservoirs (fine-grained) is proposed, and the validity of the standard is verified by the spatial correlation between the lithology probability model and the micro-seismic monitoring data. This indicated that the spatial heterogeneity of the dolomite-rich rock is the main controlling factor for the effective development of the Cenozoic continental unconventional reservoirs (fine-grained) in the Western Qaidam Basin.

Keywords: lithologic heterogeneity; rock-mechanical property; unconventional reservoirs; fine-grained; Qaidam Basin

check for updates

Citation: Li, X.; Wu, K.; Wang, J.; Yang, S.; Zhang, Q.; Zhang, Q. Impact of Lithologic Heterogeneity on Brittleness of Cenozoic Unconventional Reservoirs (Fine-Grained) in Western Qaidam Basin. *Minerals* **2022**, *12*, 1443. https://doi.org/10.3390/min12111443

Academic Editor: Luca Aldega

Received: 19 October 2022
Accepted: 10 November 2022
Published: 15 November 2022

1. Introduction

During the past decades, the increasing global consumption of hydrocarbon energy has triggered the booming of unconventional oil and gas studies. Moreover, in North America and European, the success of large-scale commercial development of shale gas from Barnett, Antrim, Marcellus, Woodford, etc. [1–5] and development of tight oil from Bakken, Eagle Ford, Wolfcamp etc. [6–11] has led to a significant unconventional oil and gas revolution, which has fundamentally reformed the global energy framework [12,13]. Since 2010, drawing on the experience of North America, China's oil and gas industry has gradually expanded its exploration targets from traditional traps to unconventional areas, realizing the economic development of marine shale gas and continental shale oil and gas in China [14].

Many scholars have promoted a further understanding on the sedimentary and reservoir characteristics, hydrocarbon generation potential and accumulation mechanism of continental fine-grained sedimentary rocks including organic-rich shale [15–19]. The continental fine-grained sedimentary rocks are quite different from conventional marine shale oil. Sedimentary rocks with a particle size of less than 0.1 mm and a content of more than 50% are generally defined as fine-grained sedimentary rocks [20]. Shale is a kind of fine-grained sedimentary rock with sheet-like or lamellar bedding structure composed of debris, clay and organic matter with a particle size of less than 0.0039 mm [17]. It is well known that a stable wide and slow tectonic setting is a necessary condition for the formation and enrichment of Marine shale oil in North America [21]. However, the continental sedimentary system in China is significantly different from the marine basin in North America in terms of basin scale, tectonic stability and sedimentary type [17]. Due to the combined influence of tectonic action, frequent provenance supply and turbulent lake level, the mixed fine-grained sedimentary rocks composed of mudstone, terrigenous clasts and carbonate minerals formed the main continental unconventional reservoirs [18,22]. The Porosity is generally less than 10% and permeability is less than 1×10^{-3} μm^2 [23,24]. The development ages of continental fine-grained sedimentary rocks range from the Upper Paleozoic Permian to the Neogene, and the sedimentary environment includes terrestrial fresh water, brackish water, salt water and alkaline water [19].

In addition to basic research on lithology, lithofacies, and source rocks in the preliminary stage, the development methods and engineering parameters of continental fine-grained sedimentary rocks are also very important. Among them, massive hydraulic fracturing has been the most effective and primary method for reservoir stimulation [23,25,26]. Variation in rock fabric and mineral compositions causes different responses of reservoirs to hydraulic fracturing, as the strain accommodation of reservoir rocks changes with lithologic types and fabric [23,24]. Therefore, it is necessary not only to accurately map the mechanical facies of the entire reservoir, but also to understand how these changes, and the properties of the reservoir rocks whose mineral composition varies greatly as a result of depositional changes.

In general, with the relative increase of clay mineral content, the limit strain that the formation can withstand before hydraulic fracturing takes effect also increases [27,28], indicating that mineral composition is the main but not all controlling factor of the mechanical properties of the reservoir rock. When the rock type changes, the strain adaptability of the formation at the buried depth may exceed its susceptibility to hydraulic fracturing. Published works indicate that previous researchers focused mainly on quantifying the mechanical properties of a particular lithology so as to understand the corresponding variables that it can withstand before failure. Therefore, strain is a key factor to quantitatively describe the mechanical behavior of rocks during the processes of hydraulic fracturing. In practice, it is often described in a variety of terms, such as ductility [27,28], brittleness [29], and hydraulic fracturability [30], etc. Among them, the term 'brittleness' has been frequently used in the evaluation of mechanical properties of unconventional reservoir rocks [31,32].

The first public discourse about a brittleness index focused on the brittle mineral components of rock [4,33,34]. Soon, the ratio of compressive strength to tensile strength was used to evaluate the brittleness of a rock, that is, the larger the ratio, the higher its brittleness [35]. With further research, the Young's modulus and Poisson's ratio were considered as two key parameters for rock brittleness characterization [29], namely, a high Young's modulus and low Poisson's ratio correspond to high brittleness [5,29,36]. Moreover, the effect of pore fluid on the mechanical properties of rock was also widely discussed—pore fluid increases the plasticity of rock and reduces brittleness [37–39]. At present, rock brittleness is comprehensively defined, generally through the evaluation of rock fracture characteristics, rock mineral composition, rock mechanical properties and pore fluid [32]. Comprehensive application of multiple methods promotes the accuracy of rock brittleness evaluation, such as rock mechanics analysis of rock samples, log data calculation and 3D seismic data inversion, etc. [29,40,41].

In any case, stress–strain characteristics and mineral composition are still the most important indicators of brittleness. In the triaxial stress test of rocks, the stress–strain curve is divided into pre-peak and post-peak stages. The pre-peak stage generally represents the stable state, while the post-peak stage refers to an unstable state due to cracks [39]. The post-peak sharp drop behavior represents significant brittleness [42]. A series of brittle–plastic models have been used to study the post-peak stress drop in rocks and to describe instability after failure. The stress drop coefficient is also an important index to evaluate the brittleness [43,44]. Previous studies on continental fine sediments were mostly based on changes in mineral composition or single mechanical properties, and lacked systematic examples of petrophysical experiments, mineral composition analysis, microscopic morphology and seismic lithology prediction. The evaluation of rock brittleness is inherently complicated, and the complexity of continental mixed fine-grained sedimentary rocks undoubtedly increases the difficulty of evaluation of brittleness. In this paper, the internal relationship between mineral compositions, rock fabric and mechanical properties is systemically studied, and conclusions will provide guiding references on the choice of reservoirs for hydraulic fracturing and engineering.

2. Geological Setting

The Qaidam Basin is a large continental intermountain hydrocarbon-bearing basin in northwest China, with ~12 $\times$ 10^4 km^2 of sedimentary rocks distributed in the basin (Figure 1a). The basin is dominated by Cenozoic strata, and seismic exploration data show that their maximum thickness is more than 10,000 m. Since the Early Cenozoic, the orogenic activities of the Eastern Kunlun Mountains and Altun Mountains have resulted in the migration of the depositional center of the Qaidam Basin from the west to the east [45,46]. The western areas are an important oil and gas rich region in the Qaidam Basin, and are our main research area (Figure 1b). The Cenozoic strata in the study area were subdivided into five stratigraphic units based on lithology, paleontology, paleomagnetism, etc. They are the Lulehe formation ($E_{1\text{-}2}l$), the Xiaganchaigou formation ($E_{2\text{-}3}xg$), the Shangganchaigou formation (E_3-N_1sg), the Xiayoushashan formation (N_1xy), and the Shangyoushashan formation (N_1sy) (Figure 1c, Table 1).

The Upper Member of the Xiaganchaigou formation ($E_{2\text{-}3}xg^2$) is the target stratum of this study, which deposited in a saline lacustrine environment and is further subdivided into a marginal (shore) sub-environment and a pelagial sub-environment [47]. The main sedimentary environment in the study area ($E_{2\text{-}3}xg^2$) is the pelagial sub-environment, which is characterized by typical mixed fine-grained sedimentary rocks (Figure 1b). The latter are characterized by high-frequency interbedded organic-rich laminated shale and carbonate [19]. In addition, terrigenous clastic materials carried by the extra buoyancy provided by the saline water contribute to the complex mineral compositions of the local carbonate rocks. The core samples in the study area are mainly migmatites of carbonate, mudstone and evaporite, including some clastic rocks of gravity flow origin. The main pore type in target layers is inter-crystalline pores formed by dolomitization, while the other pore types (such as inter-granular pores, dissolution pores, etc.) were less developed [15]. Considering the area as a series of reservoirs, reservoir matrix porosity is extremely low due to the fine-grained character and strong heterogeneity of the mixed fine-grained sedimentary rocks. The statistical results of analysis data show that the distribution peaks of porosity and reservoir permeability are 3.1%~11.5% and 0.05~0.62 μm^2, respectively [15]. All these disadvantages result in the area having a low or complete absence of natural reservoir production capacity, challenging the viability of its anthropogenic stimulation. The red rectangle in Figure 1b is the study area, which is a typical lacustrine mixed fine-grained sedimentary rock. The study of this area is of great significance to reveal the characteristics of the unconventional reservoirs (fine-grained).

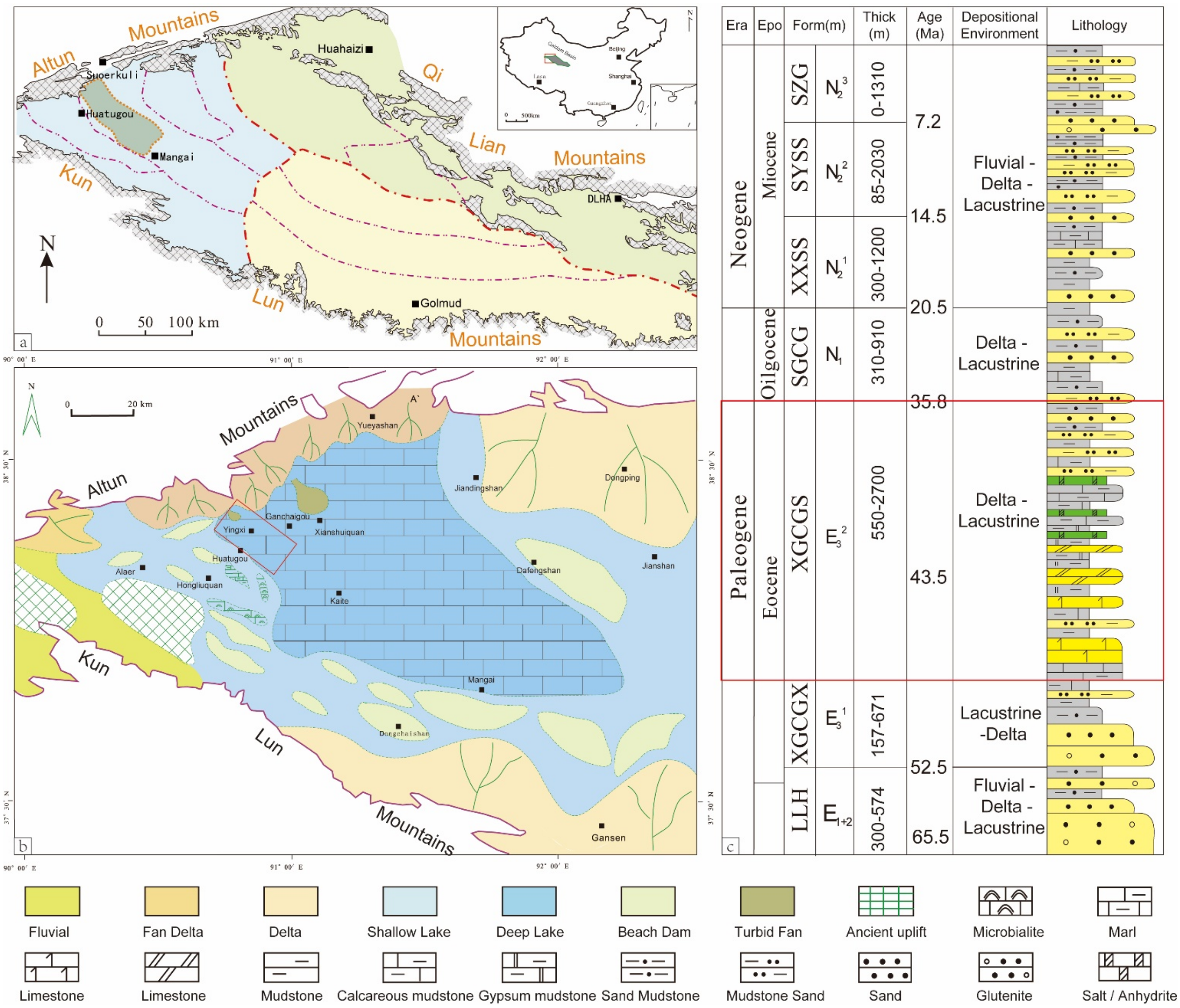

Figure 1. Tectonic location and topography of the study area in the Western Qaidam Basin: (**a**) tectonic division of the Qaidam Basin; (**b**) topography of the study site; and (**c**) comprehensive histogram of strata and lithology.

Table 1. Stratigraphy division of Cenozoic strata in the Qaidam Basin.

Stratigraphic System				Symbol	Lithology
System	**Series**	**Formation**	**Member**		
Neogene	Miocene	Shangyoushashan		N_1sy	Predominated by brown-yellow sandy mudstone, with some argillaceous siltstone and conglomerate interbeds.
		Xiayoushashan		N_1xy	Red-brown mudstone and sandy mudstone, with some brown-red siltstone and calcareous mudstone interbeds.
		Shangganchaigou		E_3-N_1sg	Gray mudstone and siltstone develop in the lower part, while the upper part is predominated by brown-yellow mudstone and fine sandstone.
Paleogene	Oligocene	Xiaganchaigou	Upper	$E_{2\text{-}3}xg^2$	Predominated by dark-grey argillaceous-lime dolostone, lime dolostone, dolomitic limestone and calcareous mudstone, some anhydrite-rich beds and halite beds develop in the upper part.
	Eocene		Lower	$E_{2\text{-}3}xg^1$	Brown-red mudstone with some grey-white fine sandstone and calcareous mudstone interbeds.
	Paleocene	Lulehe		$E_{1\text{-}2}l$	The brown-red conglomerate, conglomeratic sandstone, sandstone with some mudstone and sandy mudstone interbeds.

3. Sampling, Data Preparation and Methodology

In order to understand the impact of lithologic heterogeneity on the mechanical properties of the unconventional reservoirs (fine-grained), two groups of parallel rock samples (10 in each group) with different mineral compositions and fabrics were selected from drilling cores at a depth of 3860–4210 m in the Upper Member of Xiaganchaigou Formation. All samples were drilled using a 2.5 cm diameter core bit and then cut into cylindrical plugs ~5 cm in length. The first group of parallel samples was initially used for a triaxial stress experiment, after which they were examined by X-ray diffraction analysis. The second group of parallel samples was prepared into microscopic observation thin sections and scanning electron microscope samples.

3.1. Triaxial Experiment

Prior to analysis, the plunger samples from the first group were rinsed with the Soxhlet distillation–extraction apparatus and solvent mixture of chloroform/methanol. After 48 h of distillation–extraction, all plunger samples were then dried in an oven for 24 h. The temperature and pressure parameters for this experiment were determined from in situ measurements obtained from temperature and pressure sensors at the bottom of the well. The strata temperature of the rock samples ranges from 108~118 °C, and the confining pressure is ~50 MPa (Table 2). Taking into account the consistency with the geological conditions and the upper limit of the temperature conditions of the experimental equipment, the temperature conditions of these experiments were all set to 100 °C.

Table 2. Core plug samples and tested conditions.

Sample ID	Depth/m	Length/mm	Diameter/mm	Sectional Area/cm^2	Volume/cm^3	Cell Pressure/MPa
1-44-1	4078.37	51.28	24.79	4.83	24.75	51.03
5-47-1	4122.64	48.53	24.81	4.83	23.46	51.54
12-3-1	3860.48	48.52	24.87	4.86	23.57	48.35
8-27-1	4146.50	48.03	24.75	4.81	23.11	51.83
2-126-1	4096.66	48.37	24.72	4.80	23.21	51.24
4-1-1	4106.75	50.39	24.72	4.80	24.18	51.36
12-8-1	3861.30	46.71	24.77	4.82	22.51	48.34
16-3-1	4202.26	48.05	24.88	4.86	23.36	52.54
9-36-1	3794.30	47.17	24.76	4.81	22.71	47.47
5-6-1	3766.90	46.88	24.79	4.83	22.63	47.16

The triaxial stress tests were performed on the triaxial stress test platform of the State Key Laboratory of Oil & Gas Reservoir Geology and Exploitation Engineering of Southwest Petroleum University. The experimental equipment is RTR-1000 static/dynamic state triaxial rock mechanics servo test system of GCTS Company in the United States (Figure 2). The gray part of the experimental device shown in Figure 2b is a metal high-pressure experimental cabin, including external LVDTs, axial load, etc., while the internal rock sample fixing device is composed of top and bottom platen, porous stone and internal LVDTs. The samples were placed between the porous stone at the top and bottom. The porous stone between top platen and rock sample is used to ensure the stability of the top platen under cyclic pressure fluctuation during the experiment. In the triaxial test, when the deformation rate signal fed back by the rock sample is inconsistent with the predetermined signal, the servo controller generates a corresponding comparison signal to push the servo to change the oil supply model, ensuring the deformation rate remains in a controllable range. When the rock samples begin to rupture, the deformation process shows a decrease in the bearing capacity and an increase in the deformation rate. As the deviator stress reaches the tensile strength limit of the rock samples, the servo controller will actively close the servo valve to reduce the oil supply and rock test pressure. Thus, the test system will overcome the bursting phenomenon and obtain the specific deformation information.

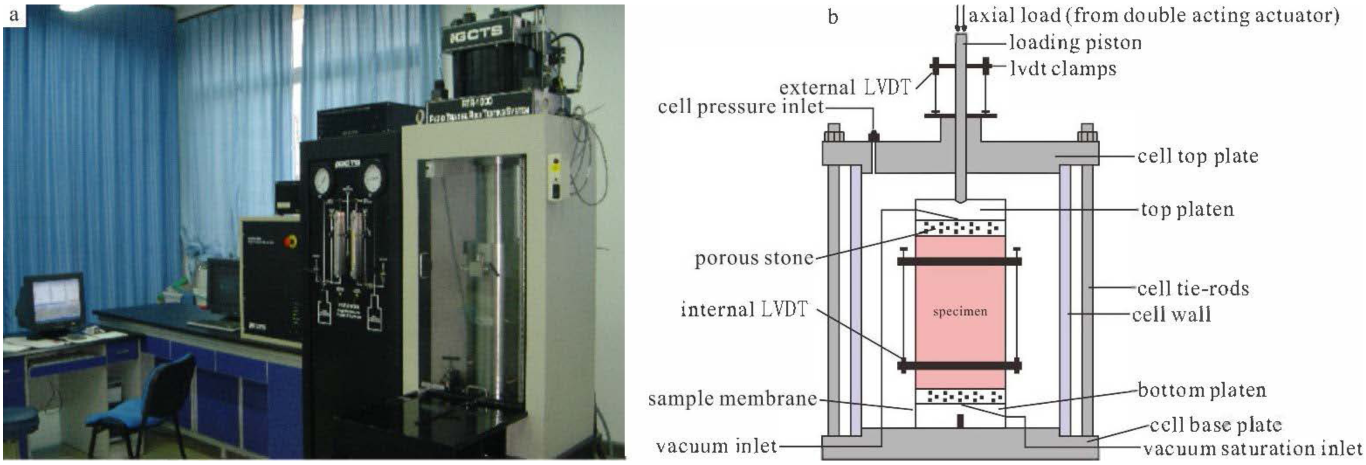

Figure 2. Triaxial stress test system (**a**) and the structure of the experiment instrument (**b**). The experimental device adopts the triaxial test in lateral isobaric mode (Photos of experimental equipment and schematic diagram of experimental devices are provided by the State Key Laboratory of Oil & Gas Reservoir Geology and Exploitation Engineering of Southwest Petroleum University).

3.2. X-ray Diffraction (XRD) Test and Petrographic Analysis

After systemically completing the triaxial stress test on all the rock samples, the mineral composition of the plunger samples was analyzed by XRD. The analysis procedure was as follows: (1) crushing—1~2 g rock samples was crushed into particles with diameter <1 mm; (2) milling—sample particles were milled to <40 μm using a grinder with agate grinding elements in a jar; (3) tablet preparation—the rock powder was placed on an aluminum sample rack on a glass plate, and the sample powder was compressed into tablets; (4) analysis—mineral composition was analyzed by Bruker D4 Endeavor diffractometer (Bruker Corporation, Billerica, MA, USA).

The fabric and micromorphological characteristics of the rock samples were analyzed by polarized microscope (PM) and scanning electron microscope (SEM). The PM used in this study is an Axio Scope-A1microscope manufactured by Carl Zeiss Microimaging GmbH (Singapore). All samples were milled into thin sections of 0.03 mm thickness prior to analysis. The SEM used in this study is Quanta 450 FEG manufactured by the FEI Company (Hillsboro, OR, USA). The pre-experiment procedure for SEM analysis was as follows: (1) the samples were cleaned with Soxhlet distillation–extraction apparatus and solvent mixtures of chloroform/methanol for 48 h; (2) all samples were dried in the oven for 24 h after cleaning; (3) fresh sections were cut on all sample axes and evenly sprayed with gold.

All the experiments were carried out at the Key Laboratory of Reservoir Description of China National Petroleum Corporation (CNPC), Beijing, China.

3.3. Microscopic and Ultra-Microscopic Morphological Analysis

The samples from the second group were prepared into thin sections and small samples cut in cross section with a diameter of 1 cm. Ten thin sections were prepared so as to observe their inner structures, notably of the types of carbonate and evaporite grains found, using a polarizing microscope (Zeiss Axio Scope A1). Further high-resolution observations of the microbialites were performed using a field-emission scanning electron microscope (FE-SEM; FEI Quanta 450 FEG) equipped with an energy dispersive spectroscope (EDS; Oxford Instruments, Abingdon-on-Thames, UK). Ten rock cubes with fresh surfaces were spattered with Au coating before the SEM observations following the method of Li et al. [48,49].

4. Results

4.1. Analytical Results

The XRD analytical results show that a total of eight different minerals were detected in the reservoir rocks in the Upper Member of the Xiaganchaigou Formation, and the mineral composition of the samples varies quite considerably (Table 3). The carbonate minerals (calcite + siderite + dolomite) are the most abundant in the samples 1-44-1, 5-47-1, 12-3-1 and 12-8-1, ranging from 40.00% to 56.60%; anhydrite is the predominant mineral in samples 2-126-1, 4-1-1 and 16-3-1, with a content of 47.30% to 55.50%; and samples 8-27-1, 5-6-1 and 9-36-1 are dominated by clastic and clay minerals. According to the mineral composition of the reservoir, the rock types can be subdivided into three types—carbonate rock, sulphate rock and argillaceous rock.

Table 3. Mineral composition and triaxial experiment results of samples.

Sample	Lithology	Depth	Q	F	Cal	Sid	Dol	Anh	Py	Clay	Young's Modulus	Elastic Limit	Peak Stress	Poisson's Ratio
		m	%								MPa			
1-44-1	Anhydrite dolomite	4078.37	9.70	4.90	9.10	0.90	36.90	38.50	nd.	nd.	43,278.20	174.26	348.51	0.34
5-47-1	Anhydrite dolomite	4122.64	5.70	8.60	8.80	0.80	46.80	14.60	6.10	8.50	37,515.00	180.69	361.39	0.27
12-3-1	Dolomite	3860.48	8.20	5.50	19.40	10.80	26.40	16.40	2.10	11.20	37,965.80	156.00	311.99	0.36
8-27-1	Argillaceous dolomite	4146.50	16.70	12.20	6.30	11.00	21.80	2.10	4.70	25.30	33,328.90	141.06	282.64	0.35
2-126-1	Anhydrite dolomite	4096.66	5.60	3.10	nd.	nd.	35.70	55.50	nd.	nd.	37,191.00	131.02	262.04	0.38
4-1-1	Anhydrite dolomite	4106.75	8.20	10.40	7.00	1.60	14.70	55.00	nd.	3.10	35,145.70	125.66	251.32	0.22
12-8-1	Anhydrite argillaceous dolomite	3861.30	9.20	7.70	12.20	1.20	26.60	29.20	2.00	11.90	32,191.70	123.15	246.30	0.37
16-3-1	Anhydrite dolomite	4202.26	6.10	9.00	nd.	nd.	26.10	47.30	2.60	8.70	32,399.10	137.80	275.59	0.38
9-36-1	Argillaceous dolomite	3794.30	15.70	6.50	0.90	8.00	19.50	13.50	3.80	32.00	23,921.70	87.45	174.90	0.22
5-6-1	Argillaceous dolomite	3766.90	22.70	12.80	17.70	nd.	17.10	4.10	4.40	21.30	21,812.50	73.65	147.31	0.27

"nd."—no data; Q—quartz; F—feldspar; Cal—calcite; Sid—siderite; Dol—dolomite; Anh—anhydrite; Py—pyrite.

In addition to the mineral analysis results, the triaxial test results reveal the variation among the samples of their geomechanical properties with mineral composition (Table 3). As two widely used brittleness parameters [5,29,36], the Young's Modulus and Poisson's ratio of reservoir rocks in the Upper Member of the Xiaganchaigou Formation range from 21,812.50 to 43,278.20 MPa and 0.22 to 0.38, respectively. The peak stress or so-called failure limit of samples is 147.31~361.39 MPa, and the elastic limit is 50% of the peak stress referring the national standard published by the Ministry of Housing and Urban-Rural Development of the People's Republic of China [50].

4.2. Stress–Strain Curves

The stress–strain curves of the reservoir rock in the triaxial stress test not only reflect the relationship between stress and strain during compaction and deformation, but also reveal various mechanical properties of the rocks [51,52]. Although many rocks exhibit coupled elastoplastic damage behavior, there are still large differences in mechanical properties between different rocks [53]. The stress–strain curves of the test samples exhibit different characteristics, and were subdivided into O, A, B, C, D, E according to their shapes and stress threshold points (Figure 3) as described by Zhou et al. [54] and Xiong et al. [55] for different stages of stress–strain curves: the crack closure stage (O–A), linear elastic stage (A–B), stable crack growth stage (B–C), unstable crack growth stage (C–D), and the stress relief stage (D–E) after the failure limit point D. The rock samples were classified into five types according to the curve shape and corresponding stress threshold (Figure 3; Table 3). Type I composed of samples 5-47-1 and 1-44-1 is characterized by a high failure limit of ~350 MPa and no O–A stage, indicating that the natural fractures are not widely developed within the rock samples (Figure 3a,b). The type of stress–strain curve is similar to the failure model for elastic–plastic materials proposed by Vincent [56]. Type II is represented by samples 12-3-1 and 8-27-1 (Figure 3c,d), whose failure limits are much lower (311.9 and 288.64 MPa, respectively). Another distinctive feature of Type II is that the stress–strain curves exhibit a periodic stress drop pattern after the failure limit, indicating that this type of reservoir rock is in a pulse failure mode of plastic materials [56]. The samples 2-162-1 and 4-1-1 are classified as the Type III, which is characterized by a similar shape to the type I curve but with a much lower failure limit. (Figure 3e,f). The shape of the stress–strain curves of samples 16-3-1, 12-8-1 and 9-36-1 show mixed characteristics of Type I, Type II and Type III, and they belong to Type IV. Their curves show elastic–plastic failure features, while the curves in the post-peak region demonstrate very weak impulse failure characteristics (Figure 3g–i). Sample 5-6-1 represents the fifth type (Type V) with completely different characteristics from the other samples (Figure 3j), which is a typical plastic failure model [56]. The pre-peak region of the Type V curves contains four complete deformation stages, and the post-peak region shows a sharp drop in stress followed by a stable stage (Figure 3j).

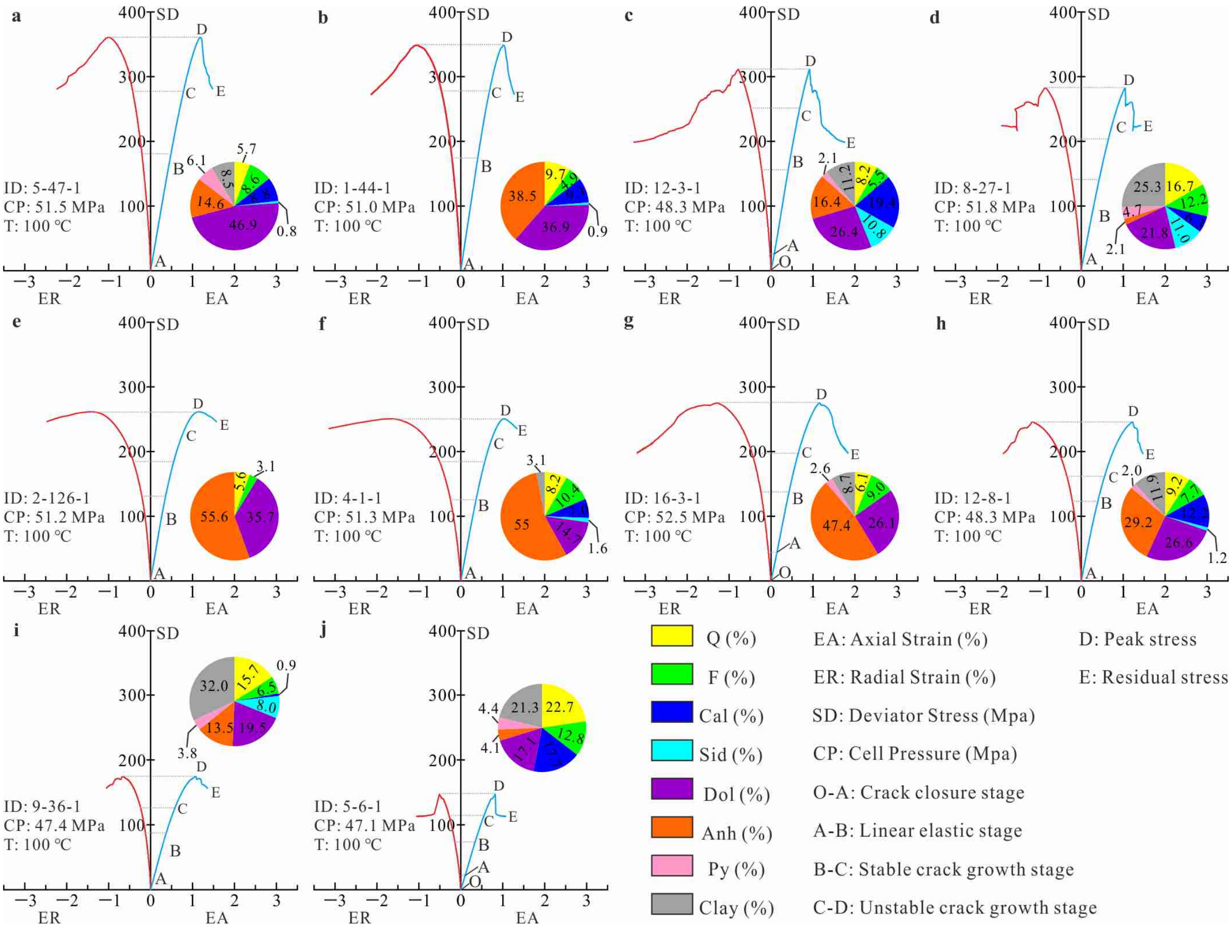

Figure 3. Diagrams of deviator stress–strain curves and the corresponding thresholds of different reservoir rocks (implications of corresponding thresholds after Zhou et al. (2018) [55] and Xiong et al. (2019) [56]). The pie charts are the results of X-ray diffraction of corresponding samples. (**a**) 5-47-1; (**b**) 1-44-1; (**c**) 12-3-1; (**d**) 8-27-1; (**e**) 2-126-1; (**f**) 4-1-1; (**g**) 16-3-1; (**h**) 12-8-1; (**i**) 9-36-1; (**j**) 5-6-1.

4.3. Petrography Analysis

Since the depositional environment of the studied strata was the depositional center of the saline lake and had undergone continuous late intense tectonic deformation [15], the reservoir morphologies are dominated by massive, bedded and laminated features. In order to understand the impact of petrography on the mechanical properties of samples, polarized microscopy (PM) and scanning electron microscopy (SEM) were used to systemically analyze the structure and texture of the rocks.

The images of PM and SEM show that the rock skeleton is mainly composed of a microcrystalline structure dominated by dolomite particles. The high-hardness framework [57] composed of a microcrystalline dolomite structure generally presents higher pressure-bearing capacity and better brittleness, while other minerals scattered throughout the rock contribute less to its strength. Meanwhile, the high strength of the rock preserves a large number of dolomitic intercrystallite pores, and these lay the foundation for good storage and fracturing stimulation capacity of this type of reservoir. There are eight test samples with porphyritic texture in the test, accounting for 80% of the total. These porphyritic samples were composed of different fabrics, resulting in significant differences in mechanical properties.

According to the stress–strain curves in Figure 3, the different rock samples were classified into five categories. Among them, Type I samples (5-47-1 and 1-44-1) show the best brittleness properties with massive structure and porphyritic texture (Figure 4a,b). The structural feature of Type I is similar to the anhydrite-rich samples, but with a different matrix texture. The Type II samples (12-3-1 and 8-27-1) are bedded and massive in structures and are of porphyritic and sandy-micritic texture, respectively (Figure 4c,d). The stress–strain curve of sample 12-3-1 in Type I (Figure 3c) shows a crack closure stage (O–A), which does not exist in curves of 5-47-1, 1-44-1 and 8-27-1 in Type II (Figure 4a,b,d). This phenomenon is caused by the interbedded cracks revealed in the microscopic images in Figure 4c. The microscopic images of sample 8-27-1 reveal numerous scattered or bedded terrigenous silt grains (Figure 4d). The clay mineral content in Type II samples is significantly higher than that in Type I samples, indicating that the increase in the proportion of clay mineral is one of the reasons for plastic deformation of the samples. In addition, petrographic interfaces usually undergo sliding deformation after peak stress, such as the bedding plane of sample 12-3-1 and the contact interface of the silt and micrite of sample 8-27-1 (Figure 4d). These petrographic interfaces exhibit plastic deformation characteristics, which are typical of weak interfaces. Furthermore, Type II samples exhibit plastic deformation characteristics but also a strength limit second only to Type I, which may be related to their low porosity. Indeed, the negative effect of the porosity of rocks on their strength has been investigated in previous studies [58].

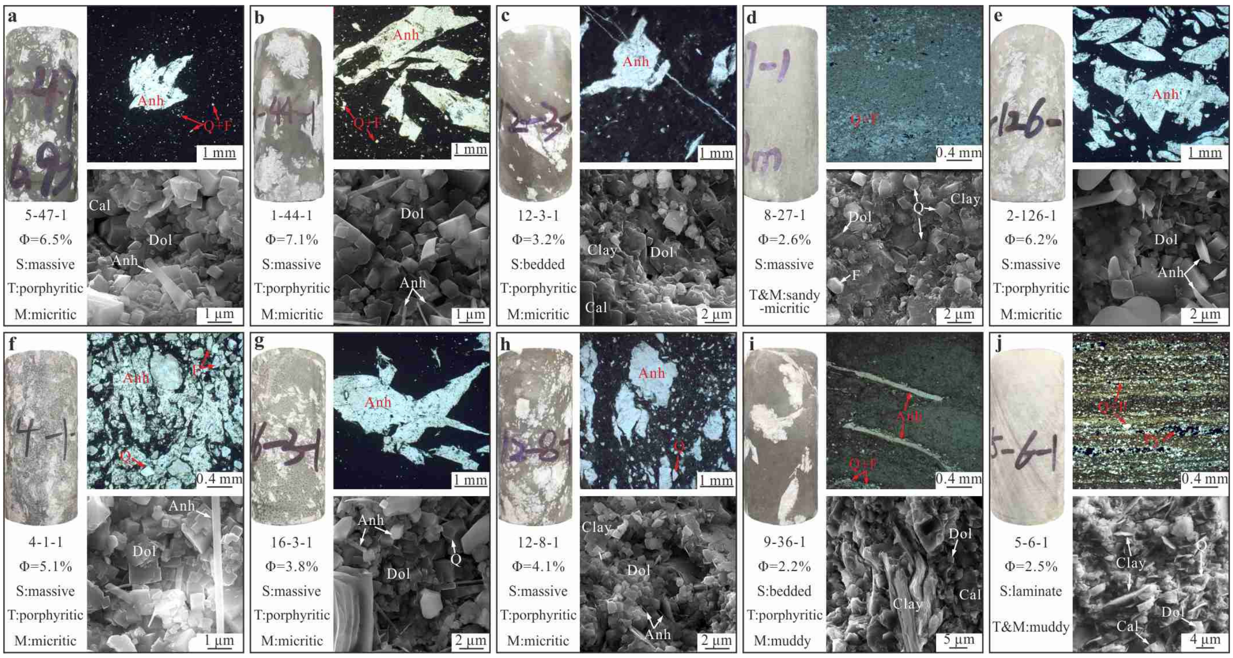

Figure 4. Petrographic charateristics of tested samples (Φ—porosity, S—structure, T—Texture, M—texture of matrix). (**a**) 5-47-1, anhydrite dolomite; (**b**) 1-44-1, anhydrite dolomite; (**c**) 12-3-1, dolomite; (**d**) 8-27-1, argillaceous dolomite; (**e**) 2-16-1, anhydrite dolomite; (**f**) 4-1-1, anhydrite dolomite; (**g**) 16-3-1, anhydrite dolomite; (**h**) 12-8-1, anhydrite argillaceous dolomite; (**i**) 9-36-1, argillaceous dolomite.; (**j**) 5-6-1, argillaceous dolomite.

5. Discussion

5.1. Inapplicability of MBI Equation

Mineral compositions of different rock samples show various trends with stress–strain types (Figure 3). Brittle rocks with high strength are usually composed of brittle minerals such as quartz, feldspar, dolomite, etc. The mineral brittleness index (MBI) has been widely used in reservoir evaluation, but its calculation equations vary according to the brittle mineral content, whether quartz, carbonate, or pyrite. (Table 4). Quartz, feldspar and carbonate minerals all have positive effects on reservoir brittleness in the equation (Table 4). On the other hand, the ductility index matches the content of ductile minerals such as clay, anhydrite, etc. [4,59,60]. The brittle mineral content (Q + F + Cal + Sid + Dol) is the driver of reservoir brittleness [61].

According to the stress–strain curves and mineral composition, type V (Figure 3j) and type II (Figure 3c,d) are the most brittle rock types, and their strain curves tend to stabilize after one or more stress drops. However, the steady state after the stress drop suggests that the fracturing of the reservoir may not be effective. In addition, the lower content of dolomite in this lithofacies combination reduces matrix porosity resulting in poor fracturing. Although the brittle mineral content, Young's modulus and failure limit (peak stress) of the 5-47-1, 1-44-1 and 12-3-1 samples are higher, the overall trend correlation between mechanical indices and the brittle mineral content is not significant (Figure 3a–c). For example, the 2-126-1 and 4-1-1 samples with higher contents such as clay or anhydrite are considered to be typical plastic minerals (Figure 3e,f) [62,63]. Therefore, the MBI equation widely used in shale reservoir brittleness evaluation is not necessarily fully applicable to continental unconventional reservoirs (fine-grained). To clarify the contribution of different minerals to reservoir brittleness, the correlation between mineral facies and mechanical properties needs to be analyzed. In addition, the occurrence state and particle size of minerals in reservoir rocks are also key factors affecting the mechanical properties of the rocks [64].

Table 4. MBI calculation equations.

Correlation for MBI	Formation	Lithology	Φ/%	TOC/%	References
$\frac{Q}{Q+Carb+Clay}$	Barnett	Shale bounded by limestone	6	1–3	Jarvie et al., 2007 [4]
$\frac{Q+Dol}{Q+Dol+Cal+Clay+TOC}$	Barnett	Shale bounded by limestone	6	1–3	Wang and Gale, 2009 [65]
$\frac{Q+Cal+Dol}{Q+Cal+Dol+Clay+TOC}$	Neuquén Basin, Argentina	Mudstones	8	2.5–3.5	Glorioso and Rattia, 2012 [61]
$\frac{Q+F+M+Carb}{tot}$	Barnett	Shale bounded by limestone	6	1–3	Jin et al., 2014 [59]

Carb—carbonate; M—mica; TOC—total organic carbon; tot—total weight fraction.

5.2. Correlation between Mineral and Mechanical Properties

Brittle minerals are the main controlling factor for rock brittleness, while ductile minerals are the opposite [4,59]. The natural properties of minerals indicate that brittle minerals have higher hardness (Table 5). The most ideal brittle minerals are quartz and feldspar, followed by carbonate minerals (dolomite and calcite), while sulfate minerals and clay minerals (harder than talc) are not conducive to the rock brittleness. Under this assumption, the mineral content of quartz and feldspar in a brittle reservoir should be relatively higher. However, the stress–strain curve in Figure 3 shows that the mechanical properties of mixed fine-grained sedimentary rocks in the study area are more complicated than assumed. Figure 4 shows the binary fitting results of different minerals and mechanical properties of the reservoir rocks.

Table 5. Mineralogical information of common rock-forming minerals.

Mineral	Chemical Formula	Crystal System	Cleavage	Mohs Hardness	Microhardness /GPa	References
talc	$Mg_3Si_4O_{10}(OH)_2$	monoclinic	perfect {001}	1	0.14 ± 0.03	Broz et al., 2006 [66]
gypsum	$CaSO_4{\cdot}2H_2O$	monoclinic	perfect {010}, good {100}	2	0.61 ± 0.15	
anhydrite	$CaSO_4$	orthorhombic	perfect {010}, good {001}	2–3	1.32 ± 0.13	Brace, 1960 [67]
calcite	$CaCO_3$	trigonal	perfect {1010}	3	1.49 ± 0.11	Broz et al., 2006 [66]
dolomite	$CaMg(CO_3)_2$	trigonal	perfect {1011}, perfect {1011}	3.5–4	3.35 ± 0.33	Wong and Bradt, 1992 [57]
orthoclase	$KAlSi_3O_8$	monoclinic	perfect {001}, good {010}	6	6.87 ± 0.66	Broz et al., 2006 [66]
quartz	SiO_2	trigonal	none	7	12.2 ± 0.61	

The comparison results of X-ray diffraction and triaxial stress tests revealed that the content of dolomite was positively correlated with Young's modulus and peak stress, with fitting ratios (r^2) of 0.69 and 0.57, respectively (Figure 5a–c). The results further exhibit that the stiffness and strength of the reservoir rock are positively related with the dolomite content. The intersection curve of dolomite content and Poisson's ratio is characterized by an upward concave (r^2 = 0.79). When the dolomite content is greater than ~30%, the Poisson's ratio is significantly negatively correlated with dolomite content (Figure 5b), while the Poisson's ratio decreases with the increase in Young's modulus. According to the criteria proposed by Rickman et al. [29] and Labani and Rezaee [36], this type of reservoir rock sample is typical of brittle reservoir rock.

On the other hand, the quartz and feldspar—two brittle minerals widely considered to be of high hardness [4,59]—were negatively correlated with Young's modulus and peak stress, respectively (Figure 5d,f, Table 5). Poisson's ratio shows a very weak negative correlation with the content of quartz and feldspar, indicating that the content of quartz and feldspar in mixed fine-grained sedimentary rocks with mixed characteristics contributes little to rock brittleness. These phenomena are inconsistent with the prevailing view of the relationship between rock mechanical properties and mineral composition, suggesting that the total content of brittle minerals may not be the only driver of the brittleness of the reservoir rocks in the study area. It is often reported that petrographic properties affect mechanical properties [68]. Therefore, the controlling effect of the internal structure and texture on the mechanical properties of the rock needs to be further explored.

The low correlation between anhydrite content and mechanical properties suggests that this type of mineral has little effect on rock brittleness (Figure 5g–i). The clay mineral content has a negative binary correlation with the mechanical properties (Figure 5j–l), indicating that reservoir brittleness is compromised with increasing clay content. By contrast, it is well known that the clay content in typical shale oil reservoirs usually does contribute more to brittleness [17]. The brittleness and ductility characteristics of samples with high clay content mainly depend on the way their particles are supported. The special contact relationship between clay particles can effectively enhance the ductility of the rock skeleton, while the stratified structure of clay in shale can reduce its static Poisson ratio.

To sum up, the content of dolomite and clay showed a correlation with mechanical properties, which is consistent with the general opinion. Mineral composition is not a simple controlling factor of rock mechanical properties, and analysis of rock petrographic characteristics (such as fabric) may be a necessary condition to understand the controlling factors of rock brittleness.

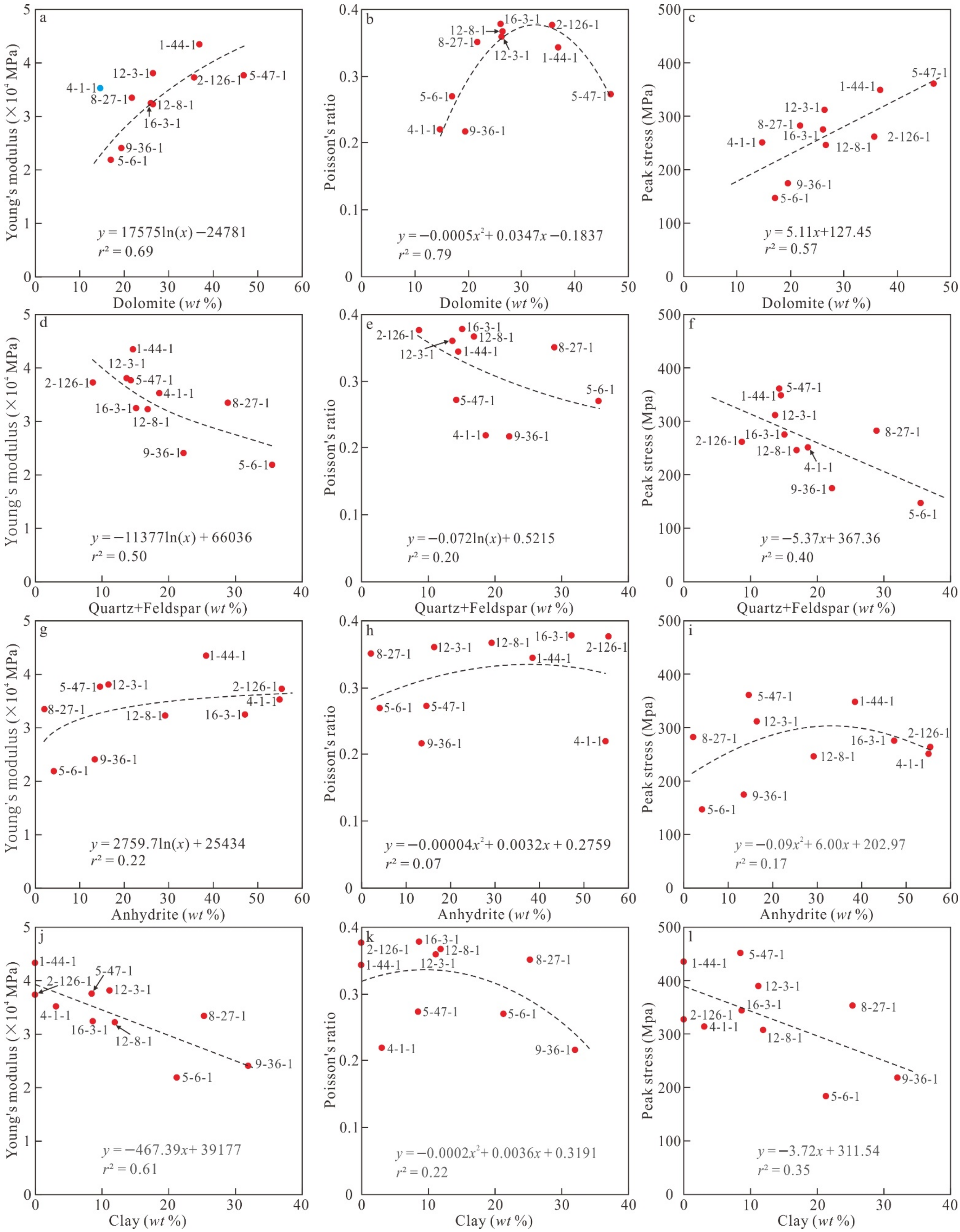

Figure 5. (**a**–**l**) Correlations between mineral content and mechanical properties. (The blue point in Figure 5a does not participate in the fitting.)

5.3. Mineralogical Impact on Mechanical Property

Rock samples with different morphologies show different mechanical properties, which are mainly controlled by the grain characteristics and combinations forming the rock skeleton. Based on the similar dolomitic skeleton, the Type III samples (2-162-1 and 4-1-1) have similar petrographic characteristics to the Type I samples (Figure 4e,f). The difference in stress strength between the two types may be caused by the anhydrite content, of which the softer anhydrite constitutes a much higher proportion in Type III than in Type I (Figure 4e,f).

The samples 16-3-1, 12-8-1 and 9-36-1 are classified as the Type IV according to the stress–strain curve shapes, which shows mixed characteristics of Type I, Type II and Type III (Figure 3). This phenomenon was caused by the combination of mineral composition and rock fabrics. The mineral composition of the Type IV samples varies widely, and the lower clay minerals of the 16-3-1 and 12-8-1 samples determine their brittleness better than the 9-36-1 sample (Figure 3, Table 3). Furthermore, the petrographic characteristics of these samples are also different, with samples 16-3-1 and 12-8-1 presenting massive structure and porphyritic texture (Figure 4g,h). Although some fine-grained terrigenous detritus and clays are present, a higher proportion of dolomite particles can still form the rock skeleton, resulting in a strength limit similar to that of type III. The high proportion of clay minerals in the 9-36-1 sample cannot form a solid framework except for the layered structure (Figure 4i), showing strong ductility.

The sample 5-6-1 belongs to Type V, which is characterized by a laminated structure and muddy texture (Figure 4i). The higher content of clay minerals and laminated petrographic characteristics are favorable for the development of many weak interfaces in the rock, contributing to a significant ductile deformation characteristic under the compressional conditions.

In summary, the samples with massive structure and dolomite matrix skeleton are more brittle than the samples with layered structure (bedded and laminated) and lack of dolomite skeleton.

5.4. Standard of Reservoir Brittleness Classification and Practical Effect

The discussion of different rock brittleness and controlling factors in the reservoir rock revealed that mineral composition and heterogeneity are of great significance to the evaluation of its geomechanical characteristics and stimulation potential. Therefore, based on the results of the triaxial compression experiments and the petrographic analyses, a comprehensive local standard of reservoir brittleness classification has been suggested to guide stimulation engineering (Table 6). The standard classifies the reservoir rocks in the study area into three grades: good, medium and poor. Brittle oil reservoirs are usually characterized by high Young's modulus and low Poisson's ratio, which are negatively correlated [5,29,36]. The correlation between mineral composition and mechanical properties reveals that when the proportion of the dolomite is higher than ~30%, Young's modulus demonstrates a negative correlation with Poisson's ratio (Figure 5b), indicating brittle reservoirs. Combined with petrographic characteristics, the presence of high-content dolomite, low-content clay, massive structure and dolomite skeleton reflects good reservoirs. Considering the storage capacity of hydrocarbon and the impact of pores on rock mechanics, the porosity of this type of reservoir is usually greater than 6%. The other two grades (medium and poor) of reservoir brittleness evaluation criteria are also defined in Table 6, including parameters such as mineral content, petrology, mechanical properties and porosity. All the tested samples are divided into 3 groups, according to the present standard, as follows: the good samples are 1-44-1, 5-47-1 and 2-126-1; the medium samples are 12-3-1, 12-8-1 and 16-3-1; and the poor samples are 8-27-1, 2-126-1, 4-1-1, 9-36-1 and 5-6-1.

Table 6. Local standard of reservoir brittleness classification.

Grade	Mineral Composition (%)		Petrography		Mechanics (MPa)		Porosity (%)
	Dolomite	Clay	Structure	Skeleton Texture	Young's Modulus	Peak Stress	
good	>30	<10	massive	micritic	>37,000	>260	≥6.0
medium	20–30	<20	massive/bedded	micritic	>32,000	>240	≥3.5
poor	<20	<40	massive/bedded/laminated	argillaceous	>20,000	>140	≥1.0

In order to prove the rationality of the standard, the stimulation effect and brittleness characteristics of heterogeneous reservoirs in the study area were revealed through lithology model and microseismic monitoring results of horizontal well volume fracturing (Figure 6). Warmer colors in the lithology model mean higher dolomite content and better brittleness (Figure 6). In practical applications, the density and intensity of micro-seismic events are usually recognized as an indicator of the fracturability of the reservoir; while microseismic detection is used to record the density and intensity of seismic events after single-well hydraulic fracturing, representing the occurrence of brittle reservoir stimulation. The micro-seismic events and lithology model of the reservoirs show a good spatial correlation (Figure 6b,c). The fracturing stages 1, 2, 5, 6, and 7 (Figure 6b,c,f) triggered more and stronger micro-seismic events than did stages of 3 and 4, which is in accordance with the distribution of the dolomite. The consistent result of brittleness and reservoir stimulation provides a good practical case for studying the impact of lithologic heterogeneity on reservoir brittleness.

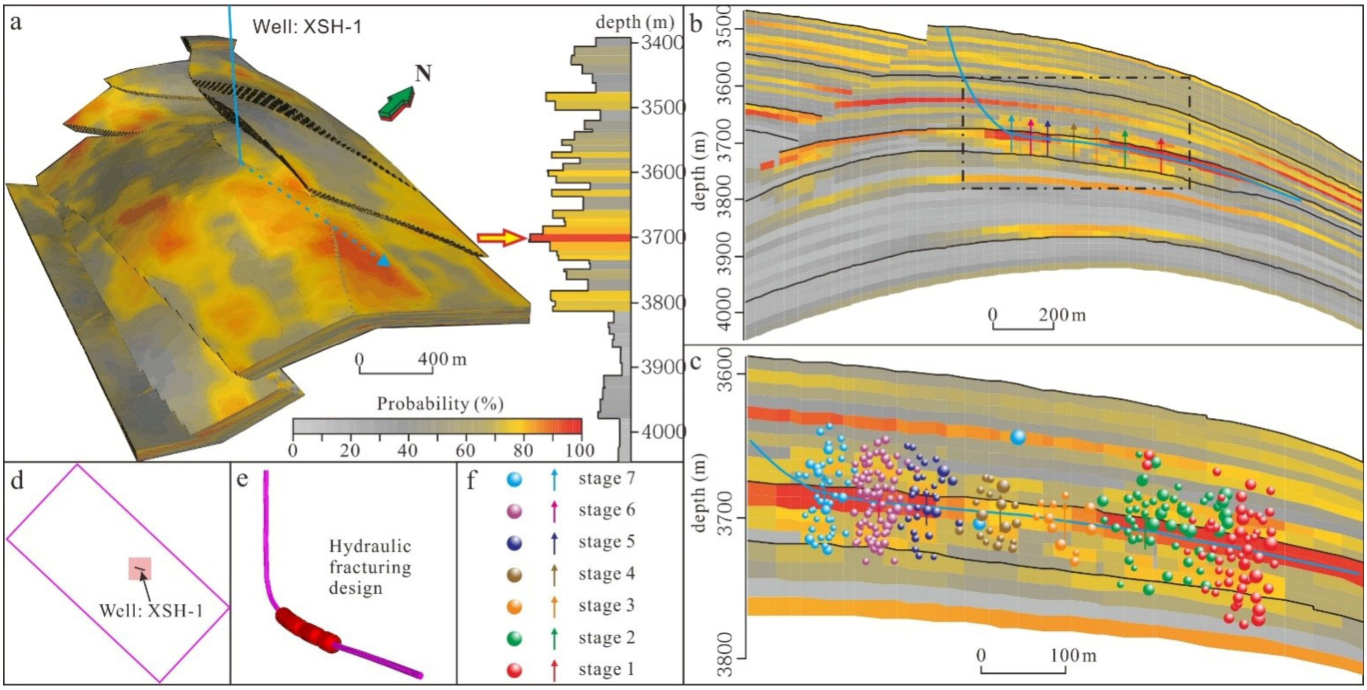

Figure 6. The micro-seismic monitoring data and lithology probability model of a stimulated horizontal well: (**a**) The 3D probability model of the distribution of good reservoirs; (**b**) profile of the probability model; (**c**) micro seismic event points of the hydraulic fracture, enlargement of the dashed outlined-box in (**b**); (**d**) well location; (**e**) well trajectory and hydraulic fracturing design; (**f**) the micro seismic event and fracturing location of each stage (indicated by the colored balls and arrows, the size of the ball indicating the strength of the seismic event in (**c**)).

6. Conclusions

After a comprehensive discussion of the triaxial compression experiment and the petrography of the reservoir rocks in the Upper Member of the Xiaganchaigou Formation in the western Qaidam Basin, knowledge of the mechanical properties and their controlling factors of unconventional reservoirs (fine-grained) is summarized as follows:

(1) The shape of stress–strain curves and the corresponding stress thresholds suggest that the tested samples can be subdivided into five types with different mechanical properties. The stress–strain curve characteristics of both Type I and Type III specimens are elastoplastic failure modes, but the failure limit of the Type I specimens is higher than that of the Type III specimens. The samples of Type II show a special pulse failure mode of the plastic material. The stress failure mode of Type IV samples shows a mix of Type I, Type II, and Type III characteristics, although their failure limit varies significantly. However, Type V shows a typical plastic failure model.

(2) The correlation between minerals and mechanical properties indicates that the widely used MBI equations are not completely applicable to the studied stratum. The commonly recognized brittle minerals such as quartz and feldspar have no obvious positive correlation with the mechanical properties which characterize the brittleness in unconventional reservoirs (fine-grained). The dolomite and clay minerals show good positive and negative correlations, respectively, with the mechanical properties of brittleness in unconventional reservoirs (fine-grained). The micro-seismic events and dolomite distribution in the lithology model of the reservoirs show a good spatial correlation. The continuous deformation after the peak and the dolomite skeleton with developed intercrystalline pores are the main indicators of the brittleness and effectiveness of these unconventional reservoirs (fine-grained).

(3) The result of petrographic analysis proves the contribution of dolomite to the rock brittleness, and confirms that dolomite particles constitute the rock skeleton of the unconventional reservoirs (fine-grained). In addition, the high hardness of the dolomite skeleton preserves a significant amount of intercrystallite pores while resisting high compressive stress, thus playing a positive role in hydrocarbon preservation. Lithofacies with lower dolomite content cannot readily form a strong rock skeleton, so its brittleness and storage capacity of the rock are relatively low.

(4) Based on our understanding of the studied strata, a set of brittleness evaluation standards for unconventional reservoirs (fine-grained) was determined, and the validity of the standards was verified by the spatial correlation between the stimulated horizontal well microseismic monitoring data and lithology probability models.

Author Contributions: X.L. contributed to the conception and organized the manuscript of the study; K.W. performed the experiment; J.W. and S.Y. contributed significantly to analysis and manuscript preparation; Q.Z. (Qinghui Zhang) and Q.Z. (Qiang Zhang) helped perform the analysis with constructive discussions. All authors have read and agreed to the published version of the manuscript.

Funding: This research was supported by CNPC "14th Five-Year" forward-looking fundamental major science and technology projects (Grant No. 2021DJ2205).

Acknowledgments: We are grateful to the four anonymous reviewers, for their constructive and helpful comments on the manuscript. We also thank the Jixin Deng for assisting the stress analysis, and Xiucheng Tan for providing helpful information on the microscopic characteristics of carbonates.

Conflicts of Interest: No conflict of interest exits in the submission of this manuscript, and manuscript is approved by all authors for publication. I would like to declare on behalf of my co-authors that the work described was original research that has not been published previously, and not under consideration for publication elsewhere, in whole or in part. All the authors listed have approved the manuscript that is enclosed.

References

1. Curtis, J.B. Fractured shale-gas systems. *AAPG Bull.* **2002**, *86*, 1921–1938.
2. Montgomery, S.L.; Jarvie, D.M.; Bowker, K.A.; Pollastro, R.M. Mississippian Barnett shale, Fort Worth basin, north-central Texas: Gas-shale play with multi-trillion cubic foot potential. *AAPG Bull.* **2005**, *89*, 155–175. [CrossRef]
3. Wilczynski, P.M.; Domonik, A.; Lukaszewski, P. Brittle Creep and Viscoelastic Creep in Lower Palaeozoic Shales from the Baltic Basin, Poland. *Energies* **2021**, *14*, 4633. [CrossRef]

4. Jarvie, D.M.; Hill, R.J.; Ruble, T.E.; Pollastro, R.M. Unconventional shale-gas systems: The Mississippian Barnett Shale of north-central Texas as one model for thermogenic shale-gas assessment. *AAPG Bull.* **2007**, *91*, 475–499. [CrossRef]
5. Grieser, W.V.; Bray, J.M. Identification of production potential in unconventional reservoirs. In Proceedings of the Production and Operations Symposium, Oklahoma City, Oklahoma, USA, 31 March–3 April 2007; Society of Petroleum Engineers: Houston, TX, USA, 2007.
6. Montgomery, S.L. Permian "Wolfcamp" limestone reservoirs; Powell Ranch Field, eastern Midland Basin. *AAPG Bull.* **1996**, *80*, 1349–1365.
7. Sonnenberg, A.S.; Pramudito, A. Petroleum geology of the giant Elm Coulee field, Williston Basin. *AAPG Bull.* **2009**, *9*, 1127–1153. [CrossRef]
8. Kuhn, P.P.; Primio, R.D.; Hill, R.; Lawrence, J.R.; Horsfield, B. Three-dimensional modeling study of the low-permeability petroleum system of the Bakken Formation. *AAPG Bull.* **2012**, *10*, 1867–1897. [CrossRef]
9. Hentz, T.F.; Ambrose, W.A.; Smith, D.C. Eaglebine play of the southwestern East Texas basin: Stratigraphic and depositional framework of the Upper Cretaceous (Cenomanian-Turonian) Woodbine and Eagle Ford Groups. *AAPG Bull.* **2013**, *12*, 2551–2580. [CrossRef]
10. Fairbanks, M.D.; Ruppel, S.C.; Rowe, H. High-resolution stratigraphy and facies architecture of the Upper Cretaceous (Cenomanian-Turonian) Eagle Ford Group, Central Texas. *AAPG Bull.* **2016**, *3*, 379–403. [CrossRef]
11. Aderibigbe, A.; Valdes, C.C.; Heidari, Z. Integrated rock classification in the Wolfcamp Shale based on reservoir quality and anisotropic stress profile estimated from well logs. *Interpretation* **2016**, *4*, SF1–SF18. [CrossRef]
12. Yergin, D. *The Quest: Energy, Security, and the Remaining of the Modern World*; Penguin Press: London, UK, 2011; pp. 1–300.
13. EIA. *Technically Recoverable Shale Oil and Shale Gas Resources: An Assessment of 137 Shale Formations in 41 Countries Outside the United States*; U.S. Energy Information Administration: Washington, DC, USA, 2013; pp. 1–150.
14. Li, G.X.; Luo, K.; Shi, D.L. Key technologies, engineering management and important suggestions of shale oil/gas development: Case study of a Duvernay shale project in Western Canada Sedimentary Basin. *Pet. Explor. Dev.* **2020**, *47*, 791–802. [CrossRef]
15. Zhang, S.; Cao, Y.C.; Zhu, R.K.; Xi, K.L.; Wang, J.; Zhu, N.; Hu, R.N. Lithofacies classification of fine grained mixed sedimentary rocks in the Permian Lucaogou Formation, Jimsar sag, Junggar Basin. *Earth Sci. Front.* **2018**, *25*, 198.
16. Deng, Y.; Pu, X.G.; Chen, S.Y.; Yan, J.H.; Shi, Z.N.; Zhang, W.; Han, W.Z. Characteristics and controlling factors of fine-grained mixed sedimentary rocks reservoir: A case study of the 2nd member of Kongdian formation in Cangdong depression, Bohai Bay basin. *J. China Univ. Min. Technol.* **2019**, *48*, 1301–1316.
17. Li, M.W.; Ma, X.X.; Jiang, Q.G.; Li, Z.M.; Pang, X.Q.; Zhang, C.T. Enlightenment from formation conditions and enrichment characteristics of marine shale oil in North America. *Pet. Geol. Recovery Effic.* **2019**, *26*, 13–28.
18. Zhou, L.; Chen, C.; Han, G.; Yang, F.; Ma, J.; Zhou, K.; Zhang, W.; Huang, C. Geological Characteristics and Shale Oil Exploration Potential of Lower First Member of Shahejie Formation in Qikou Sag, Bohai Bay Basin. *Earth Sci.* (In Chinese with English Abstract). **2019**, *44*, 2736–2750.
19. Li, X.; Li, F.; Wang, J.; Wang, B.; Wang, Z.; Sun, X.; Yi, C. Formation and preservation of Eocene lacustrine microbialites in the western Qaidam Basin (northeastern Qinghai-Tibetan Plateau, China): Petrological, mineralogical, and geochemical constraints. *Sediment. Geol.* **2022**, *440*, 106257. [CrossRef]
20. Zou, C.N.; Zhang, G.S.; Yang, Z.; Tao, S.Z.; Hou, L.H.; Zhu, R.K.; Wang, Z.P. Geological concepts, characteristics, resource potential and key techniques of unconventional hydrocarbon: On unconventional petroleum geology. *Pet. Explor. Dev.* **2013**, *40*, 385–399. [CrossRef]
21. Tyson, R.V.; Pearson, T.H. Modern and ancient continental shelf anoxia: An overview. *Geol. Soc. Lond. Spec. Publ.* **1991**, *58*, 1–24. [CrossRef]
22. Zhou, S.; Xia, C.; Zhou, Y. A theoretical approach to quantify the effect of random cracks on rock deformation in uniaxial compression. *J. Geophys. Eng.* **2018**, *15*, 627–637. [CrossRef]
23. Bodziak, R.; Clemons, K.; Stephens, A.; Meek, R. The role of seismic attributes in understanding the hydraulically fracturable limits and reservoir performance in shale reservoirs: An example from the Eagle Ford Shale, south Texas. *AAPG Bull.* **2014**, *98*, 2217–2235. [CrossRef]
24. Dong, T.; Harris, N.B.; Ayranci, K.; Yang, S. The impact of rock composition on geomechanical properties of a shale formation: Middle and Upper Devonian Horn River Group shale, Northeast British Columbia, Canada. *AAPG Bull.* **2017**, *101*, 177–204. [CrossRef]
25. Bustin, A.M.M.; Bustin, R.M. Importance of rock properties on the producibility of gas shales. *Int. J. Coal Geol.* **2012**, *103*, 132–147. [CrossRef]
26. Sone, H.; Zoback, M.D. Mechanical properties of shale-gas reservoir rocks-Part 1: Static and dynamic elastic properties and anisotropy. *Geophysics* **2013**, *78*, D381–D392. [CrossRef]
27. Donath, F.A. Some information squeezed out of rock. *Am. Sci.* **1970**, *58*, 54–72.
28. Ferrill, D.A.; Morris, A.P. Fault zone deformation controlled by carbonate mechanical stratigraphy, Balcones fault system, Texas. *AAPG Bull.* **2008**, *92*, 359–380. [CrossRef]
29. Rickman, R.; Mullen, M.; Petre, E.; Grieser, B.; Kundert, D. A practical use of shale petrophysics for stimulation optimization: All shale plays are not clones of the Barnett Shale. In Proceedings of the SPE Annual Technical Conference and Exhibition, Denver, Colorado, USA, 21–24 September 2008; SPE-115258-MS.

30. Enderlin, E.M.; Bartholomaus, T.C. Sharp contrasts in observed and modeled crevasse patterns at Greenland's marine terminating glaciers. *Cryosphere* **2020**, *14*, 4121–4133. [CrossRef]
31. Geng, Z.; Chen, M.; Jin, Y.; Yang, S.; Yi, Z.C.; Fang, X.; Du, X.Y. Experimental study of brittleness anisotropy of shale in triaxial compression. *J. Nat. Gas Sci. Eng.* **2016**, *36*, 510–518. [CrossRef]
32. Li, Z.; Li, L.; Li, M.; Zhang, L.; Zhang, Z.; Huang, B.; Tang, C. A numerical investigation on the effects of rock brittleness on the hydraulic fractures in the shale reservoir. *J. Nat. Gas Sci. Eng.* **2018**, *50*, 22–32.
33. Bishop, A.W. Progressive failure with special reference to the mechanism causing it. In Proceedings of the Geotechnical Conference, Oslo, Norway; 1967; Volume 2, pp. 142–150.
34. Buller, D.; Hughes, S.N.; Market, J.; Petre, J.E.; Spain, D.R.; Odumosu, T. Petrophysical evaluation for enhancing hydraulic stimulation in horizontal shale gas wells. In Proceedings of the SPE Annual Technical Conference and Exhibition Society of Petroleum Engineers, Florence, Italy, 19–22 September 2010.
35. Hucka, V.; Das, B. Brittleness determination of rocks by different methods. *Int. J. Rock Mech. Min. Sci. Geomech. Abstr.* **1974**, *11*, 389–392. [CrossRef]
36. Labani, M.M.; Rezaee, R. The importance of geochemical parameters and shale composition on rock mechanical properties of gas shale reservoirs: A case study from the Kockatea shale and Carynginia formation from the Perth basin, Western Australia. *Rock Mech. Rock Eng.* **2015**, *48*, 1249–1257. [CrossRef]
37. Heidari, M.; Khanlari, G.R.; Torabi, K.M. Effect of Porosity on Rock Brittleness. *Rock Mech. Rock Eng.* **2014**, *47*, 785–790.
38. Paul, S.; Sun, C.C. Lubrication with magnesium stearate increases tablet brittleness. *Powder Technol.* **2017**, *309*, 126–132. [CrossRef]
39. Tan, W.H.; Ba, J.; Guo, M.Q.; Li, H.; Zhang, L.; Yu, T.; Chen, H. Brittleness characteristics of tight oil siltstones. *Appl. Geophys.* **2018**, *15*, 175–187. [CrossRef]
40. Goodway, B.; Varsek, J.; Abaco, C. Practical applications of P-wave AVO for unconventional gas Resource Plays. *CSEG Rec.* **2006**, *31*, 52–65.
41. Mullen, M.J.; Roundtree, R.; Turk, G.A. A composite determination of mechanical rock properties for stimulation design (what to do when you don't have a sonic log). In Proceedings of the SPE Rocky Mountain Oil & Gas Technology Symposium, Denver, CO, USA, 16–18 April 2007; SPE-108139-MS.
42. Tarasov, B.; Potvin, Y. Universal criteria for rock brittleness estimation under triaxial compression. *Int. J. Rock Mech. Min. Sci.* **2013**, *59*, 57–69. [CrossRef]
43. Ge, X.R. Post failure behavior and a brittleplastic model of brittle rock. In *Computer Methods and Advances in Geomechanics*; AA Balkema Publishers: London, UK, 1997; pp. 151–160.
44. Shi, G.C.; Ge, X.R.; Lu, Y.D. Experimental study on coeffi cients of brittle stress drop of marble. *Chin. J. Rock Mech. Eng.* **2006**, *25*, 1625–1631.
45. Lu, H.; Xiong, S. Magnetostratigraphy of the Dahonggou section, northern Qaidam Basin and its bearing on Cenozoic tectonic evolution of the Qilian Shan and Altyn Tagh Fault. *Earth Planet. Sci. Lett.* **2009**, *288*, 539–550.
46. Fu, S.; Ma, D.; Chen, Y.; Zhang, G.; Wu, K. New advance of petroleum and gas exploration in Qaidam Basin. *Acta Pet. Sin.* **2016**, *37*, 1–10.
47. Wang, J.G.; Zhang, D.W.; Yang, S.Y.; Li, X.; Shi, Y.J.; Cui, J.; Zhang, P.; Wang, Y.L.; Yi, D.H.; Chang, H.Y. Sedimentary characteristics and genesis of the salt lake with the upper member of the Lower Ganchaigou Formation from Yingxi sag, Qaidam basin. *Mar. Pet. Geol.* **2020**, *111*, 135–155. [CrossRef]
48. Li, F.; Yan, J.; Algeo, T.; Wu, X. Paleoceanographic conditions following the end-Permian mass extinction recorded by giant ooids (Moyang, South China). *Glob. Planet. Chang.* **2013**, *105*, 102–120. [CrossRef]
49. Li, F.; Yan, J.X.; Burne, R.V.; Chen, Z.Q.; Algeo, T.J.; Zhang, W.; Tian, L.; Gan, Y.L.; Liu, K.; Xie, S.C. Paleo-seawater REE compositions and microbial signatures preserved in laminae of Lower Triassic ooids. *Palaeogeogr. Palaeoclimatol. Palaeoecol.* **2017**, *486*, 96–107. [CrossRef]
50. Ministry of Housing and Urban-Rural Development of the People's Republic of China. *Standard for Test Methods of Engineering Rock Mass (GB/T 50266-2013)*; China Planning Press: Beijing, China, 2013; p. 91.
51. Meng, Z.; Zhang, J.; Peng, S. Influence of sedimentary environments on mechanical properties of clastic rocks. *Environ. Geol.* **2006**, *51*, 113–120.
52. Zhao, Y.; Zhou, H.; Zhong, J.; Liu, D. Study on the relation between damage and permeability of sandstone at depth under cyclic loading. *Int. J. Coal Sci. Technol.* **2019**, *6*, 479–492.
53. Shao, J.F.; Jia, Y.; Kondo, D. An Elastoplastic Damage Model for Unsaturated Argillites. In *Elsevier Geo-Engineering Book Series*; Elsevier: Amsterdam, The Netherlands, 2004; pp. 495–500.
54. Zhou, L.H.; Pu, X.G.; Chen, C.W.; Yang, F.; Xia, J.; Guan, Q.S.; Huang, C.Y. Concept, Characteristics and Prospecting Significance of FineGrained Sedimentary Oil Gas in Terrestrial Lake Basin: A Case from the Second Member of Paleogene Kongdian Formation of Cangdong Sag, Bohai Bay Basin. *Earth Sci.* **2018**, *43*, 3625–3639, (In Chinese with English Abstract).
55. Xiong, L.; Wu, S.; Zhang, S. Mechanical Behavior of a Granite from Wuyi Mountain: Insights from Strain-Based Approaches. *Rock Mech. Rock Eng.* **2019**, *52*, 719–736. [CrossRef]
56. Vincent, J.F.V. *Structural Biomaterials*; The Macmillan Press: London, UK, 1982; p. 207.
57. Wong, T.Y.; Bradt, R.C. Microhardness anisotropy of single crystals of calcite, dolomite and magnesite on their cleavage planes. *Mater. Chem. Phys.* **1992**, *30*, 261–266.

58. Palchik, V.; Hatzor, Y.H. The influence of porosity on tensile and compressive strength of porous chalks. *Rock Mech. Rock Eng.* **2004**, *37*, 331–341.
59. Jin, X.; Shah, S.N.; Roegiers, J.C.; Zhang, B. An integrated petrophysics and geomechanics approach for fracability evaluation in shale reservoirs. *Soc. Pet. Eng. J.* **2015**, *20*, 518–526.
60. Mathews, H.L.; Schein, G.; Malone, M. Stimulation of gas shales: They're all the same-right? In Proceedings of the SPE Hydraulic Fracturing Technology Conference, College Station, Texas, USA, 29–31 January 2007; pp. 29–31.
61. Glorioso, J.C.; Rattia, A. Unconventional reservoirs: Basic petrophysical concepts for shale gas. In *SPE/EAGE European Unconventional Resources Conference & Exhibition-from Potential to Production, Vienna, Austria, 20–22 March 2012*; European Association of Geoscientists & Engineers: Houten, The Netherlands, 2012.
62. Zouaoui, H.; Lecomte-Nana, G.L.; Krichen, M.; Bouaziz, J. Structure, microstructure and mechanical features of ceramic products of clay and non-plastic clay mixtures from Tunisia. *Appl. Clay Sci.* **2017**, *135*, 112–118.
63. Xu, L.; Gao, H.; Xu, J.; Xu, M.; Wang, X.; You, F.; Long, Y. Experimental insights into a novel over-saturated brine cement slurry used in anhydrite formation. *Bulg. Chem. Commun.* **2017**, *49*, 214–219.
64. Hudson, J.A.; Harrison, J.P. *Engineering Rock Mechanics, Part 1: An Introduction to the Principles*; Elservier Ltd.: Oxford, UK, 1997; p. 429.
65. Wang, F.P.; Gale, J.F.W. Screening Criteria for Shale-Gas Systems. 2009. Available online: https://archives.datapages.com/data/gcags_pdf/2009/wanggale.htm (accessed on 18 October 2022).
66. Broz, M.E.; Cook, R.F.; Whitney, D.L. Microhardness, toughness, and modulus of Mohs scale minerals. *Am. Mineral.* **2006**, *91*, 135–142. [CrossRef]
67. Brace, W.F. Behavior of rock salt, limestone, and anhydrite during indentation. *J. Geophys. Res.* **1960**, *65*, 1773–1788. [CrossRef]
68. Räisänen, M. Relationships between texture and mechanical properties of hybrid rocks from the Jaala–Iitti complex, southeastern Finland. *Eng. Geol.* **2004**, *74*, 197–211. [CrossRef]